Validation of Postinjection Transmission Measurements for Attenuation Correction in Neurological FDG-PET Studies

Patrick K. Hooper, Steven R. Meikle, Stefan Eberl and Michael J. Fulham
PET Department, Division of Medical Imaging Services, Royal Prince Alfred Hospital, Sydney, Australia

Accurate estimation of local cerebral metabolic rate of glucose utilization (LCMRGlu) with PET requires a separate measurement of photon attenuation using a transmission source that extends study duration. The feasibility of postinjection transmission (PIT) scanning has been demonstrated but not previously validated in humans. **Methods:** Preinjection and postinjection transmission scans were performed in 26 patients undergoing routine [^{18}F]fluorodeoxyglucose (FDG) neurological PET. The PIT data were processed with two methods: One estimated emission contamination using an independent emission scan (PIT_{ind}); the other estimated the contamination directly from the PIT scan, using simultaneously acquired emission data for subtraction (PIT_{sim}). These methods were compared with measured attenuation correction (AC) using preinjection transmission data (AC_{pre}) and calculated AC (AC_{calc}). After reconstruction, image data were reformatted to fit a standard brain atlas to facilitate analysis of the region of interest and to allow subtraction of datasets averaged over all subjects. **Results:** The ratios of LCMRGlu values with respect to those obtained by the AC_{pre} method ranged from 0.98 to 1.06 (mean ± s.d., 1.01 ± 0.02) for PIT_{ind}, from 0.96 to 1.04 (mean 0.99 ± 0.02) for PIT_{sim} and from 0.77 to 1.12 (mean 0.96 ± 0.07) for AC_{calc}. Both PIT methods agreed well with the AC_{pre} method, whereas AC_{calc} gave rise to appreciable bias in structures near thick bone or sinuses. **Conclusion:** Accurate quantitative estimates of LCMRGlu can be obtained using PIT measurements. The PIT methods shorten study duration and increase patient throughput. The PIT_{sim} method has the further advantage that it is not affected by tracer redistribution and can therefore be applied to tracers with relatively rapid kinetics in vivo.

Key Words: postinjection transmission; neurology; fluorine-18-fluorodeoxyglucose; PET; attenuation correction

J Nucl Med 1996; 37:128–136

Correction for attenuation of annihilation photons in PET critically affects the ability to accurately measure physiological processes in vivo (*1,2*). Attenuation correction (AC) is usually performed using an external (transmission) radiation source that may comprise a fixed ring or one or more rotating rod sources. A transmission scan, typically 10–20 min in duration, is performed, after which the PET tracer is administered to the patient. Depending on the tracer injected and the need for kinetic data, a single (static) frame or a dynamic emission scan of 60 min or longer may then be carried out. Static imaging with [^{18}F]2-fluoro-2-deoxy-D-glucose (FDG) requires a delay between tracer administration and data acquisition while the tracer reaches a steady state (*3*). Thus, the patient must remain motionless in the tomograph for a long period, which limits patient throughput and increases the likelihood of patient movement, with attendant inaccurate attenuation correction.

A common compromise in many clinical PET centers is the application of analytical, so-called calculated, AC, which eliminates the need for a transmission scan. The calculated method assumes uniform skull thickness and constant attenuation in the brain and skull (*4*). Such assumptions do not hold for sections that pass through sinuses and regions where the bone is much thicker (e.g., skull base and occiput) and thus may cause bias in adjacent brain regions. Alternatively, the transmission scan may be performed after tracer administration, referred to here as postinjection transmission (PIT). The feasibility of this approach has been demonstrated (*5–7*), but validation of PIT scanning in a series of patients has not previously been reported. Both calculated AC and PIT scanning markedly reduce the patient's time in the tomograph. Figure 1 illustrates duration on the PET scanner using different methods of AC.

We developed a PIT technique using a commercial positron tomograph that does not require an independent emission scan to derive AC factors. Our aims were to (a) determine whether our method was a valid alternative to the gold standard of measured attenuation correction—preinjection transmission measurements—in patient studies; (b) compare the quantitative accuracy of our method with a previously reported PIT method (*5*) and calculated AC; and (c) assess the impact of our method on patient throughput.

THEORY

Sinogram Windowing

Transmission sinogram windowing (*8–10*) is used in PIT measurements to reduce contamination of the transmission data by the emission source and by scatter. At a particular rod position, a limited number of detector pairs (lines of response [LoR]) are collinear with the rod source. The LoRs collinear with this rod source position trace out a sine wave in the sinogram used to store the data (Fig. 2). A narrow "sinogram window" is defined around the sine wave traced out by the collinear LoRs. Only LoRs within this window are stored in the transmission sinogram. The LoRs that fall outside this window are due to scattered coincidences or arise from the emission source and are discarded. This step reduces significant contamination of transmission data by scatter and the emission source.

The rod sources rotate around the patient during an actual transmission scan, which requires their positions to be continually encoded to generate sinogram windows that track the rotation of the rod sources. For a sinogram window width of seven bins and the three rod sources used in our studies, the magnitude of the contamination for typical emission count rates is about 20% of total counts for LoRs passing through the center of the brain (where transmission counts are lowest).

Postinjection Transmission Measurements

As the rods rotate, the time duration of exposure to the window is different for each LoR. Therefore, the contribution of emission events to the transmission window is not constant. Let

Received Nov. 14, 1994; revision accepted Apr. 12, 1995.
For correspondence or reprints contact: Michael J. Fulham, MD, PET Department, Royal Prince Alfred Hospital, Missenden Road, Camperdown 2050, Sydney, Australia.

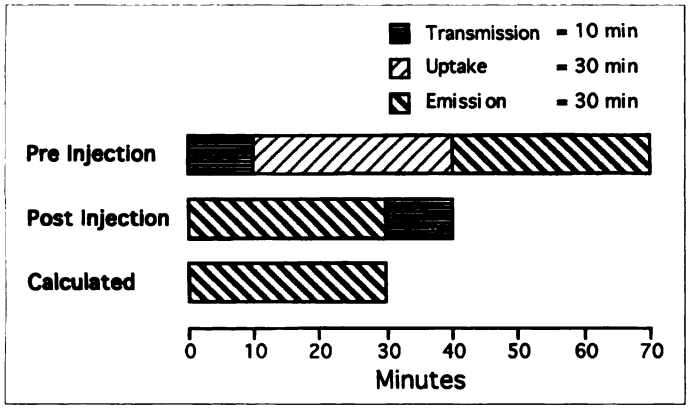

FIGURE 1. PET protocols indicating duration of patient time in the tomograph. PIT scanning eliminates need for patient to be in the tomograph during tracer uptake. Calculated AC further shortens study duration.

r_i be the relative efficiency of the ith LoR for measuring emission events, ignoring attenuation by the rods. Thus, the number of coincidences recorded within the transmission window, W^{tr}, is given by

$$W_i^{tr} = T_i + (1 - r_i)E_i, \qquad \text{Eq. 1}$$

where E_i and T_i are the number of coincidences arising from the emission and transmission sources, respectively.

The distribution of emission coincidences E_i can be derived from the latter part (e.g., last 10 min) of the independent emission scan performed immediately beforehand, taking into account differences in acquisition time and radioactive decay between the time of the two measurements. This assumes that there is no tracer redistribution between the emission and PIT scans. We denote the independent emission scan by E^{ind}. If the emission scan is acquired for t_{ind} minutes, the PIT scan is acquired for t_{pi} minutes, and the two scans are performed Δt minutes apart, the transmission component of the postinjection scan is given by:

$$T_i = W_i^{tr} - \frac{t_{pi}}{t_{ind}}(1 - r_i)E_i^{ind}e^{-\lambda\Delta t} \qquad \text{Eq. 2}$$

where λ is the decay constant for the emission radionuclide. This is equivalent to the PIT method reported previously (*5,6*). In our implementation, the last 5 min of the independent emission scan is used to estimate the emission contribution to the PIT measurement.

Alternatively, the transmission component can be derived from the postinjection measurement alone, using the simultaneously acquired emission data. Using the same definitions as before, the number of coincidences recorded in the ith LoR within the emission window is given by

$$W_i^{em} = r_iE_i + fT_i, \qquad \text{Eq. 3}$$

where f is the fraction of transmission events that spill over into the emission window (assumed constant). Equations 1 and 3 can be solved for the unknown transmission component of the postinjection scan as follows:

$$T_i = W_i^{tr} - \left\{\frac{(1 - r_i)(W_i^{em} - fW_i^{tr})}{r_i + fr_i - f}\right\}, \qquad \text{Eq. 4}$$

and both r_i and f can be measured. For example, on our scanner (ECAT 951R-CTI/Siemens, Knoxville, TN), the spillover fraction was measured as 8.6% using three rotating rods and a 7-pixel wide (22 mm) window applied to each rod. This was done by simultaneously measuring data inside and outside the transmission window when there was no emission source present. Similarly, the relative detector efficiency (r_i in Equations 1–4) was measured at every point in the sinogram by generating a uniform field of noiseless coincidence data (in software) as input to the sinogram windowing board. The values of r_i were calculated by dividing the number of emission events recorded in a given projection bin by the number of input events. The average value of r_i over the central 40 cm of the field of view was 0.93 (range 0.90–0.97).

This method, which we call PIT_{sim}, is identical in implemen-

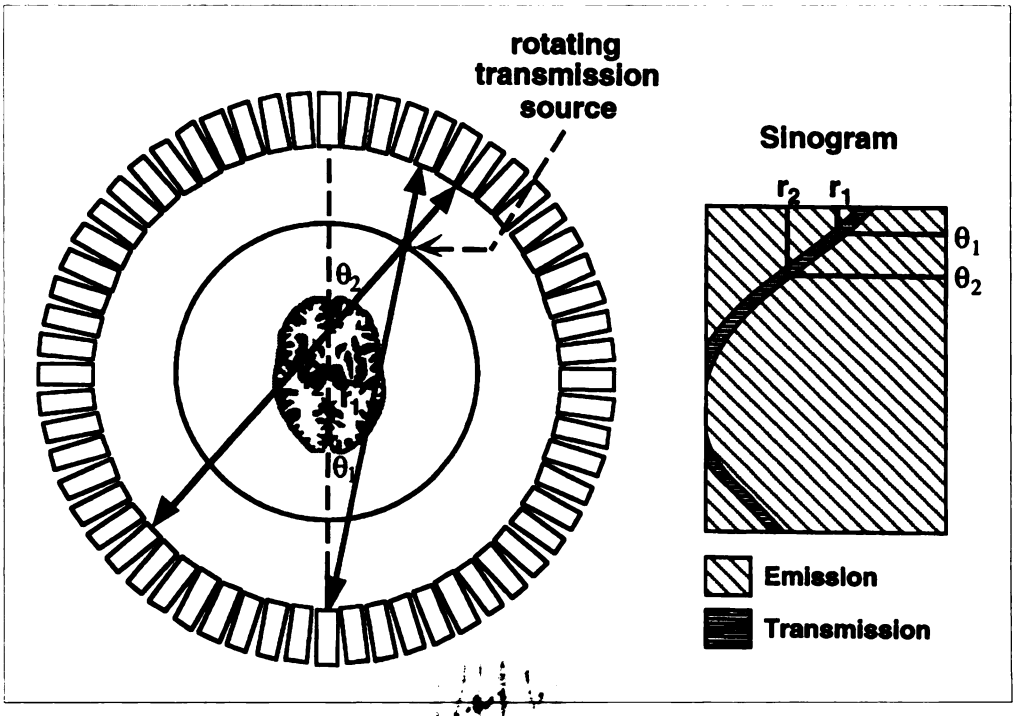

FIGURE 2. Examples of two LoRs, defined by radii r_1 and r_2 and angles θ_1 and θ_2, which are collinear with the current rod source position. The locations of the data bins in the sinogram for these LoRs are also shown. A sine wave is traced out by all LoRs passing through this rod position (transmission region). A narrow window around the sine wave is used to reject LoRs not collinear with the transmission source (emission region).

tation to a method that we previously developed and validated (*11*) for simultaneously measuring emission and transmission data in whole-body PET. In PIT scanning, however, the emission data are used for the correction step only and are then discarded.

The PIT_{sim} method has some potential advantages over the previously reported PIT approach: (a) The new method is unaffected by tracer redistribution between the emission and PIT scans, (b) Patient movement between the emission scan and the PIT scan does not affect the accuracy of the emission subtraction. Such movement, however, would affect the accuracy of AC using either method.

Conversion to Broad-Beam Attenuation Factors

In our department, preinjection transmission scans are performed without sinogram windowing, resulting in the inclusion of scatter in the measurements, or so-called broad-beam geometry. Because emission data were not corrected for scatter in the methods that follow, broad-beam attenuation correction factors (ACFs) are appropriate to use to ensure accurate quantitative values. However, because PIT necessarily involves sinogram windowing, the resulting ACFs are approximately narrow-beam, and a correction is required to yield ACFs equivalent to the preinjection method.

Let x be distance across the attenuating medium and μ_b and μ_n be the broad- and narrow-beam attenuation coefficients, respectively. On the basis of published data describing the buildup of scatter with depth for 511-keV photons (*12*), it is reasonable to assume a linear relationship between μ_b and μ_n over the range of tissue densities and thicknesses encountered in the head (i.e., $k = \mu_b/\mu_n$). Therefore, according to this assumption, narrow-beam ACFs can be related to broad-beam ACFs as follows:

$$ACF_{broad} = \exp(\mu_b x) = [\exp(\mu_n x)]^k = (ACF_{narrow})^k. \quad \text{Eq. 5}$$

In the following section, ACFs calculated using PIT data were converted to broad-beam values by Equation 5 for comparison with preinjection data. The factor k was determined by experimentation as described next.

MATERIALS AND METHODS

Instrumentation and Data Acquisition

All examinations were performed on an ECAT 951R whole-body tomograph with rod source windowing installed. The ECAT 951R uses three rotating rod sources for transmission measurements. Each rod contained approximately 50 MBq ^{68}Ge/Ga during the period that this study was undertaken. The sinogram window was seven projection bins wide (22 mm), centered on the position of each rod source as it rotated. This window width has been shown (*13*) to maximize the transmission noise equivalent count rate (NEC).

Intravenous cannulae were placed in the patient's arms, and one arm was placed in a water bath heated to 44°C to promote arteriovenous shunting (*14,15*). The patient was positioned in the scanner, and head movement was minimized with an in-house perspex restraint or a thermoplastic face mask. Throughout the examination, the patient's eyes were patched and ears plugged. Lights were dimmed in the scanning suite for the duration of the procedure. A 10 min nonwindowed transmission study was performed. After the transmission study, approximately 370 MBq of [^{18}F]FDG was administered at a constant infusion rate over a 3-min period using an automated injection pump. An emission scan was performed that consisted of 22 frames over a 60-min period from the start of tracer infusion. During the first 6 min after tracer administration, 13 blood samples were taken from the arterialized vein, and 20 samples in total were taken over the duration of the study. Immediately after the emission scan, a 10-min windowed simultaneous transmission-emission scan was performed.

Data Processing

Attenuation correction was applied to the emission data using four methods: (a) measured AC with preinjection transmission (AC_{pre}); (b) measured AC using PIT with independent emission subtraction (PIT_{ind}) [i.e., the method of Carson et al. (*5*)]; (c) measured AC using PIT with subtraction of the simultaneously acquired emission data (PIT_{sim}) and (d) calculated AC (AC_{calc}).

For measured AC, transmission and blank sinograms were first smoothed in both transaxial and axial directions using a kernel that is approximately Gaussian with an effective 15-mm FWHM. Attenuation images were reconstructed from the natural logarithm of blank-to-transmission ratios using filtered backprojection and a Shepp-Logan filter with a critical frequency (f_c) equal to the Nyquist rate (f_{Nyq} = 1.6 cycles · cm^{-1}). The extent of patient movement between preinjection and postinjection transmission scans was determined by measuring translation and rotation coefficients using a voxel-based image coregistration package (*16*). For calculated AC, commercial software (ECAT v 6.4D) was utilized which implements the method of Bergstrom et al. (*4*). Skull thickness was assumed to be 4.5 mm in all planes; the head outline was determined from emission sinograms, and μ values of 0.095 cm^{-1} for tissue and 0.151 cm^{-1} for bone were used. Correction for photon attenuation by the perspex head support was not carried out for AC_{calc} because it requires a transmission scan of the adjustable head support with the end result that the study duration would equal that of PIT. For each of the three measured methods of AC, the average of six circular regions of interest (ROIs) (diameter = 25 mm for brain, 6 mm for bone) was calculated to determine average μ values in brain and bone.

After AC, emission data were reconstructed using filtered backprojection with a Shepp-Logan filter ($f_c = f_{Nyq}$). Images were reconstructed into 128 × 128 matrices with pixel dimensions of 1.83 mm in-plane and 3.38 mm axially. Images were summed from 30 to 60 min after injection and converted to local cerebral metabolic rates of glucose utilization (LCMRGlu) using the arterialized venous input function and the autoradiographic technique (*3,14*). Population rate constants of $k_1 = 0.102$ min^{-1}, $k_2 = 0.13$ min^{-1}, $k_3 = 0.062$ min^{-1} and $k_4 = 0.0068$ min^{-1} were used, and the lumped constant was 0.418.

Calculation of Broad-Beam Correction Factor

Nonwindowed and windowed transmission scans were performed for 60 min each on a 20-cm-diameter water-filled cylinder. Attenuation images were reconstructed from the natural logarithm of the blank to transmission ratios for both the nonwindowed and windowed studies. The average of five nonoverlapping 50-mm-diameter circular ROIs placed on 10 central planes was calculated for each study. The ratio of the μ values so obtained yielded the broad-beam correction (k in Equation 5) to be applied to ACFs calculated using PIT measurements.

Patients

Twenty-six patients (12 men, 14 women; mean age 52 ± 17 yr, range 21–75 yr) undergoing routine FDG PET imaging for a range of neurologic conditions were included in this study. Indications for the functional imaging study included seizure localization in refractory epilepsy, brain tumor grading/response to treatment and dementia. Informed consent was obtained from each patient before commencement of the PET study. The studies were performed over a 4-mo period.

TABLE 1
Neurological Structures Used in ROI Analysis

Region and Structure	Label
Frontal	
Right superior frontal	rsf
Left superior frontal	lsf
Right superior mesial frontal	rsmf
Left superior mesial frontal	lsmf
Right medial lateral frontal cortex	rmlfc
Left medial lateral frontal cortex	lmlfc
Right mesial frontal	rmf
Left mesial frontal	lmf
Right orbital frontal	rof
Left orbital frontal	lof
Right gyrus rectus	rgr
Left gyrus rectus	lgr
Parietal	
Right superior parietal	rsp
Left superior parietal	lsp
Right superior mesial parietal	rsmp
Left superior mesial parietal	lsmp
Deep nuclei	
Right thalamus	rthal
Left thalamus	lthal
Right head caudate nucleus	rhc
Left head caudate nucleus	lhc
Right putamen	rput
Left putamen	lput
Occipital	
Right occipital association cortex	roac
Left occipital association cortex	loac
Right visual cortex	rvc
Left visual cortex	lvc
Right precuneus	rprc
Left precuneus	lprc
Temporal	
Right insula	rins
Left insula	lins
Right superior lateral temporal	rslt
Left superior lateral temporal	lslt
Right mesial temporal	rmt
Left mesial temporal	lmt
Right lateral inferior temporal	rlit
Left lateral inferior temporal	llit
Right inferior mesial temporal	rimt
Left inferior mesial temporal	limt
Posterior fossa	
Pons	pons
Right cerebellar hemisphere	rch
Left cerebellar hemisphere	lch
Right dentate nucleus	rdn
Left dentate nucleus	ldn
Vermis	verm

Comparison of Attenuation Correction Techniques

To compare AC techniques, irregular ROIs were placed on easily identifiable supratentorial and infratentorial cortical and subcortical structures (Table 1). Consistent and accurate placement of regions across all 26 subjects, without operator bias, was facilitated by reformatting the data to fit the standard computerized brain atlas (CBA) (*17–20*). In each patient, parameters for fitting the data to the standard atlas were determined by interactively adjusting its database regions to fit the AC_{pre} data. Because the images obtained by each of the four AC methods within a single subject are perfectly registered, the same reformat parameters were used for each of the four AC methods (AC_{pre}, both PIT and AC_{calc} methods). This also ensured that image registration before and after stereotactic normalization remained the same.

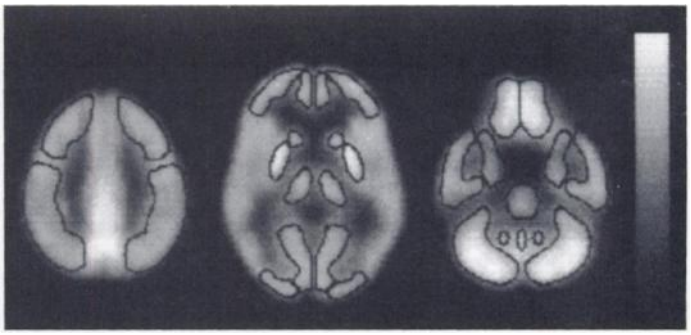

FIGURE 3. Transaxial images show average emission image obtained by the AC_{pre} method with representative irregular ROIs used in analysis of averaged patient data.

The ROIs were defined on the AC_{pre} transaxial slices averaged across all 26 patients after stereotactic normalization. Sample images and selected ROIs are shown in Figure 3. The ROIs were positioned on each reformatted patient dataset, and the mean LCMRGlu was measured in corresponding anatomic structures with each AC method. All AC methods were compared to the AC_{pre} method by calculating the ratio of LCMRGlu values for corresponding anatomic structures in each patient. For each region and AC method, mean and s.d. of the ratios were calculated. Significant differences between LCMRGlu values ($p < 0.01$) were tested using the two-tailed paired Student's t-test for each ROI. The 10.8-cm axial field of view of our PET scanner meant that structures in the most superior and inferior imaging planes were, in many cases, less well sampled than those in central planes. Slices in which ROI data were incomplete were excluded from the analysis. The number of patients sampled for each region is indicated in Table 2.

Images obtained by each of the four AC methods were averaged across all 26 patients after stereotactic normalization to generate difference images depicting systematic discrepancies between the techniques. Difference images were calculated by subtracting the AC_{pre} average images from the average images of the other three methods.

Effect on Patient Throughput

The number of patient studies that could be completed in a typical work day, using the different methods of AC, was calculated according to the following criteria:

1. The day was 8 hr in duration.
2. All studies were neurological FDG-PET studies (Fig. 1).
3. The day began with the preinjection transmission for the AC_{pre} method and the first injection for the PIT and AC_{calc} methods.
4. All patients had an injection of 370 MBq FDG.
5. Ten minutes were allowed for patient transfer/positioning.
6. Uptake period was 30 min for all patients and was conducted "off-camera" for both PIT and AC_{calc}.

RESULTS

Movement between Preinjection and Postinjection Transmission Scans

The coefficients of translation and rotation describing spatial misregistration between preinjection and postinjection transmission data are presented in Table 3. The mean and s.d. of estimated translations in the XY plane were less than 1 mm. Slightly larger translations were observed in the Z direction

TABLE 2
Ratios of LCMRGlu Values Versus Those Obtained by AC_{pre}

Region and Structure*	n†	PIT_{ind} (s.d.)	PIT_{sim} (s.d.)	AC_{calc} (s.d.)
Frontal				
rsf	22	1.00 (0.03)	0.98 (0.03)‡	0.93 (0.09)‡
lsf	22	1.00 (0.03)	0.98 (0.03)‡	0.94 (0.09)‡
rsmf	22	1.00 (0.06)	0.98 (0.05)	0.94 (0.08)‡
lsmf	22	0.99 (0.06)	0.97 (0.05)	0.95 (0.08)‡
rmlfc	26	1.01 (0.05)	1.00 (0.04)	1.00 (0.09)
lmlfc	26	1.01 (0.04)	1.00 (0.03)	1.00 (0.10)
rmf	26	1.02 (0.06)	1.00 (0.06)	1.03 (0.07)
lmf	26	1.01 (0.06)	0.99 (0.05)	1.03 (0.08)
rof	26	1.01 (0.04)	0.99 (0.04)	0.98 (0.07)
lof	26	1.01 (0.04)	0.99 (0.04)	0.99 (0.09)
rgr	22	0.98 (0.06)	0.96 (0.06)‡	1.09 (0.12)‡
lgr	22	0.99 (0.06)	0.97 (0.06)	1.12 (0.14)‡
Parietal				
rsp	22	1.00 (0.03)	0.98 (0.03)‡	0.88 (0.07)‡
lsp	22	1.00 (0.03)	0.98 (0.03)	0.87 (0.08)‡
rsmp	22	0.99 (0.03)	0.97 (0.04)‡	0.87 (0.04)‡
lsmp	22	0.99 (0.05)	0.98 (0.05)	0.87 (0.04)‡
Deep nuclei				
rthal	26	1.04 (0.08)‡	1.02 (0.07)	1.02 (0.06)
lthal	26	1.06 (0.05)‡	1.04 (0.05)‡	1.03 (0.07)
rhc	26	1.01 (0.07)	0.99 (0.08)	1.02 (0.08)
lhc	26	1.04 (0.06)‡	1.02 (0.05)	1.02 (0.06)
rput	26	1.02 (0.05)	1.00 (0.05)	0.99 (0.07)
lput	26	1.02 (0.06)	1.01 (0.06)	1.00 (0.06)
Occipital				
roac	26	1.02 (0.04)	1.01 (0.04)	0.78 (0.12)‡
loac	26	1.03 (0.05)‡	1.02 (0.04)	0.77 (0.10)‡
rvc	26	1.04 (0.05)‡	1.02 (0.05)	0.90 (0.07)‡
lvc	26	1.04 (0.04)‡	1.01 (0.03)	0.90 (0.07)‡
rprc	25	1.01 (0.06)	1.00 (0.07)	0.92 (0.05)‡
lprc	25	1.02 (0.04)‡	1.01 (0.05)	0.92 (0.06)‡
Temporal				
rins	26	1.04 (0.08)	1.02 (0.08)	1.01 (0.08)
lins	26	1.03 (0.06)	1.01 (0.06)	1.01 (0.07)
rslt	26	1.00 (0.03)	0.98 (0.03)‡	0.93 (0.07)‡
lslt	26	1.00 (0.03)	0.98 (0.08)	0.91 (0.07)‡
rmt	26	1.02 (0.09)	0.99 (0.08)	0.97 (0.10)
lmt	26	1.02 (0.08)	0.99 (0.04)	0.96 (0.08)‡
rlit	22	0.98 (0.04)	0.96 (0.04)‡	0.99 (0.08)
llit	22	0.98 (0.04)	0.96 (0.07)‡	0.99 (0.09)
rimt	22	0.98 (0.07)	0.96 (0.06)‡	1.00 (0.13)
limt	22	0.99 (0.06)	0.97 (0.08)‡	0.99 (0.08)
Posterior fossa				
pons	22	1.02 (0.08)	0.99 (0.03)	1.02 (0.07)
rch	22	1.01 (0.03)	0.99 (0.03)	0.88 (0.06)‡
lch	22	1.00 (0.03)	0.98 (0.03)	0.87 (0.05)‡
rdn	22	1.03 (0.11)	1.01 (0.11)	0.97 (0.10)
ldn	22	0.99 (0.10)	0.97 (0.10)	0.97 (0.09)
verm	22	0.99 (0.08)	0.97 (0.09)	0.94 (0.10)‡
Mean		1.01 (0.02)	0.99 (0.02)	0.96 (0.07)

*See Table 1 for structure code.
†n = number of patients contributing to ROI data.
‡$p < 0.01$.

(1.75 ± 1.08 mm), but this is still well within the slice spacing in the axial direction (3.38 mm). Two subjects had Z translations greater than the interslice spacing, but in both cases all other movements were estimated to be less than 1 mm and less than 1 degree. Similarly, the mean and s.d. of estimated rotations in all three planes were less than 1 degree. Therefore, movement between preinjection and postinjection transmission scans was considered to be minimal.

Calculation of Broad-Beam Correction Factors

The average μ values for water were 0.089 ± 0.001 cm^{-1} for the nonwindowed study and 0.093 ± 0.001 cm^{-1} for the

TABLE 3
Measured Movement between Preinjection and Postinjection Transmission Studies

	Translations (mm)			Rotations (degree)		
	x	y	z	xy	xz	yz
Mean	0.31	0.52	1.75	0.58	0.33	0.41
s.d.	0.22	0.49	1.08	0.77	0.56	0.45
Max	0.82	2.02	4.19	3.29	2.89	2.11

Max = maximum.

windowed transmission study. Thus, the broad-beam correction factor k was calculated to be 0.96.

Measured Attenuation Coefficients

The average μ values for each transmission method are presented in Table 4. Results obtained by PIT_{ind} and PIT_{sim} are in good agreement with those obtained by the AC_{pre} method after broad-beam correction. Before broad-beam correction, μ values were 5% higher in brain tissue and bone for both PIT_{ind} and PIT_{sim} when compared with those for AC_{pre}.

Average and Subtraction Images

Figure 4 shows average and difference images in the transaxial plane for the PIT_{sim} (Fig. 4A) and AC_{calc} (Fig. 4B) methods compared with those for the AC_{pre} method. There was good correspondence between LCMRGlu values using the PIT_{sim} method, with minimal discrepancies apparent in the subtraction image. However, for the AC_{calc} method, several areas of relatively increased or decreased LCMRGlu values were apparent. Relatively higher metabolic values were seen in the inferior frontal lobe. Relatively lower values were observed in superficial cortical regions, including the posterior parietal and posterior occipital lobes and both cerebellar hemispheres. Images from a patient with dementia (Fig. 5) also clearly depict relative reductions in occipital LCMRGlu values and relative increases in inferior frontal LCMRGlu values compared with those for the AC_{pre} method. In contrast, no appreciable differences were observed between the AC_{pre} and PIT_{sim} images in this patient.

Region of Interest Analysis

Ratios of average LCMRGlu values, presented in Table 2 and shown graphically in Figure 6, confirm the impressions of the images in Figures 4 A and B. The ratio of PIT_{ind} to AC_{pre} was very close to 1 in all 44 ROIs (range 0.98–1.06, mean 1.01 ± 0.02). Eight of the regions had LCMRGlu values significantly different ($p < 0.01$) from the reference values. One region (left thalamus = 1.06) had a bias greater than 5%. The results were similar using PIT_{sim} (range 0.96–1.04, mean 0.99 ± 0.02). The LCMRGlu values were significantly different in 11 of the regions. However, there were no regions that differed from the corresponding AC_{pre} regions by more than 5% (Fig. 7A). By comparison, there was considerable variation in the ratio of values obtained by the AC_{calc} method to those obtained by the AC_{pre} method (range 0.77–1.12, mean 0.96 ± 0.07) (Fig. 7B). Significant differences were observed in 22 of the 44 ROIs. In 21 of these regions, the differences between AC_{calc} and AC_{pre} were greater than 5%. The greatest differences were observed in the parietal lobe (−13%), occipital association cortex (−23%), cerebellar hemispheres (−13%) and gyrus recti (+12%).

TABLE 4
Measured μ Values for Each Attenuation Correction Method

AC method	μ values	
	Tissue (s.d.)	Bone (s.d.)
AC_{pre}	0.097 (0.002)	0.11 (0.01)
PIT_{ind}	0.102 (0.002)	0.12 (0.01)
PIT_{sim}	0.101 (0.002)	0.12 (0.01)
PIT_{ind}*	0.098 (0.002)	0.12 (0.01)
PIT_{sim}*	0.097 (0.002)	0.11 (0.01)

*After narrow-beam to broad-beam correction.

Effect on Patient Throughput

Estimated patient throughput for an 8-hr day using the AC methods described in this report was as follows: (a) For AC_{pre}, six studies can be carried out, requiring 12.5 GBq of FDG; (b) for PIT, nine studies can be performed using 16 GBq; (c) for AC_{calc}, 19.5 GBq is needed to perform 11 studies. Therefore, AC_{calc} results in the greatest patient throughput, as expected. However, PIT scanning also enables a marked increase in patient throughput (50%) compared with AC_{pre}, with the advantage that attenuation coefficients are measured and not assumed.

DISCUSSION

We described and validated two PIT methods, where one PIT technique does not require an independent emission scan to derive AC factors. Both methods were compared with calculated AC and the gold standard, measured AC, using preinjection transmission data. Our main findings were the following: (a) There was excellent agreement between LCMRGlu values derived from PIT measurements using either method and those derived from preinjection transmission data. (b) Calculated attenuation correction gave rise to significant bias in LCMRGlu values in several brain regions, ranging from −23% to +12%. (c) The PIT method markedly reduces study duration and can increase patient throughput without loss of quantitative accuracy.

We implemented the PIT methods with rotating rod sources according to the technique of Carson et al. (*5*), who compared a single rotating rod source to PIT measurements made with a ring source and reported that the rod source technique was less sensitive to changes in tracer redistribution between the emission and transmission scans. We extended this approach by introducing a technique that estimates the emission contribution directly from the PIT scan. Our method eliminates errors due to tracer redistribution and allows the possibility of performing transmission measurements during the rapid tracer uptake period before a steady state is reached. An alternative approach, described by Ranger et al. (*7*), used point sources collimated into a fan beam in the scanning plane. The technique of Ranger et al. is also insensitive to tracer redistribution because the effect of the collimation is to reduce emission contamination in the PIT measurement to a negligible level. However, this method requires significant hardware modification, whereas the rotating rod sources that we used are available on current commercial PET tomographs.

Although calculated AC methods offer greater reduction in study duration than PIT scanning, this reduction is achieved at the expense of reduced quantitative accuracy. The greatest differences between calculated AC and the preinjection transmission method were seen in areas where brain tissue is in close proximity to thick skull bones or air in the sinus cavities.

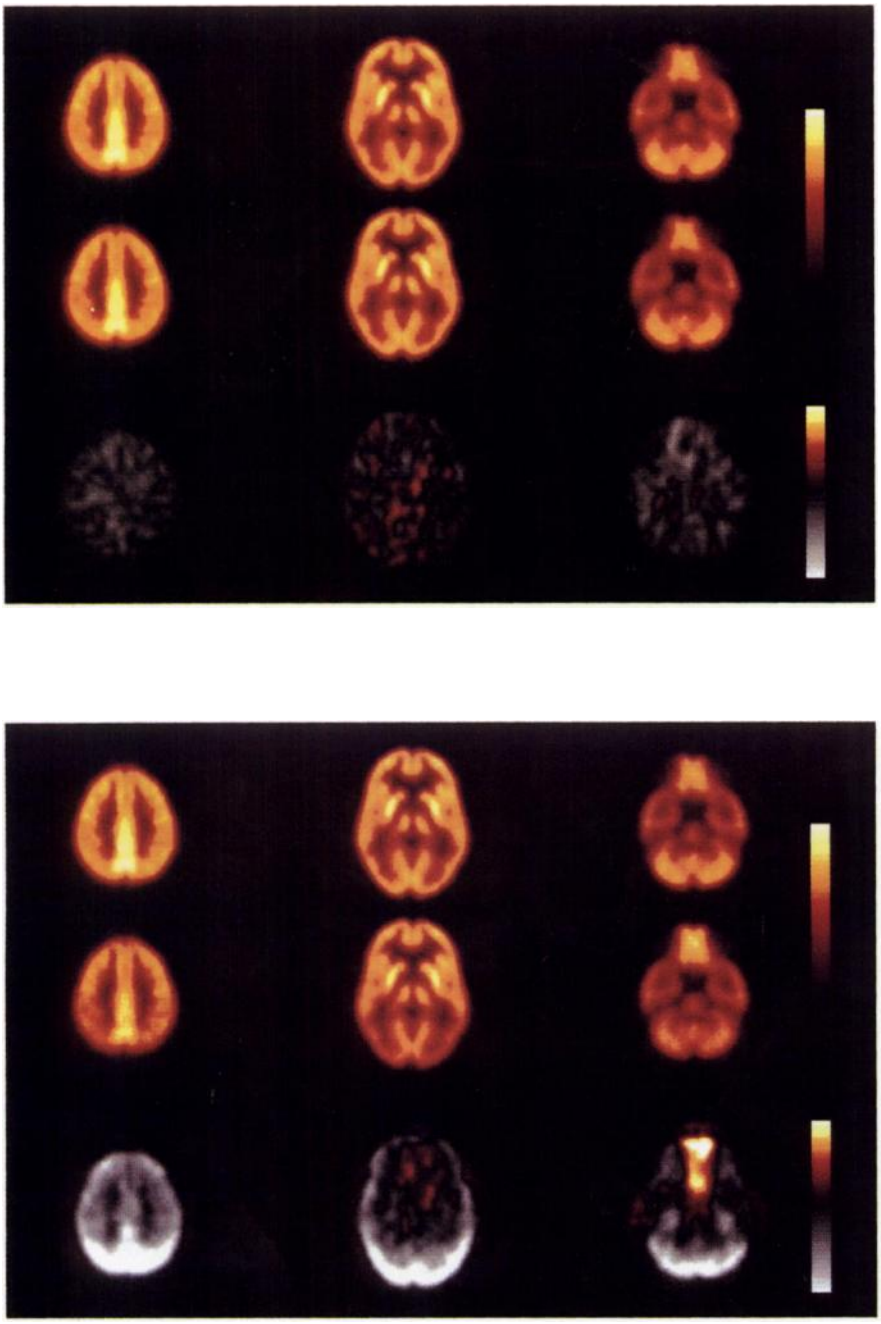

FIGURE 4. (A) Average and subtraction images comparing PIT_{sim} with AC_{pre}. (B) Average and subtraction images comparing AC_{calc} with AC_{pre}. For each panel, average images obtained by AC_{pre} are shown in top row; method being compared is shown in middle row and difference images are shown in bottom row. Color scale for bottom row is split to indicate positive differences in "hot-iron" scale and negative differences in gray scale. Difference images are windowed to a maximum absolute difference of 10%.

Glucose utilization was underestimated in the parietal lobe, posterior fossa structures and the occipital association cortex, which are all adjacent to thick bones. Photon attenuation by the perspex head support, which was not accounted for, may also have contributed to the low metabolic values observed in these regions. Conversely, the gyrus recti had increased LCMRGlu values because these structures are in close proximity to the frontal sinuses. These sites of overestimation and underestimation of glucose metabolism may compromise the interpretation of clinical PET studies in patients with cognitive impairment and epilepsy.

However, it should be noted that although preinjection measured attenuation correction is the accepted gold standard, it is an imperfect one. Preinjection measured AC includes marked smoothing of the transmission data to minimize noise propagation. Such smoothing may introduce artifacts in the corrected images in regions where attenuation changes suddenly (*21,22*). The magnitude of these artifacts is small, however, and we do not believe that the smoothing is responsible for the major differences seen between the AC_{calc} and AC_{pre} methods in our Figures 4B and 5.

There are several other technical issues raised by our study. Potential sources for error include (a) the effects of stereotactic normalization, (b) potential patient movement between transmission measurements and (c) the effect of different scatter contributions to preinjection and postinjection transmission measurements. We used stereotactic normalization to aid our comparison of the different methods and to eliminate operator error in the placement of ROIs. To ensure that ROI analysis was not affected by the accuracy of the fit to the CBA, we used the same transformation parameters for each of the four AC methods within each patient. The slight loss in resolution introduced by the trilinear interpolation during transformation has a negligible effect on the ROI values. The transformation is

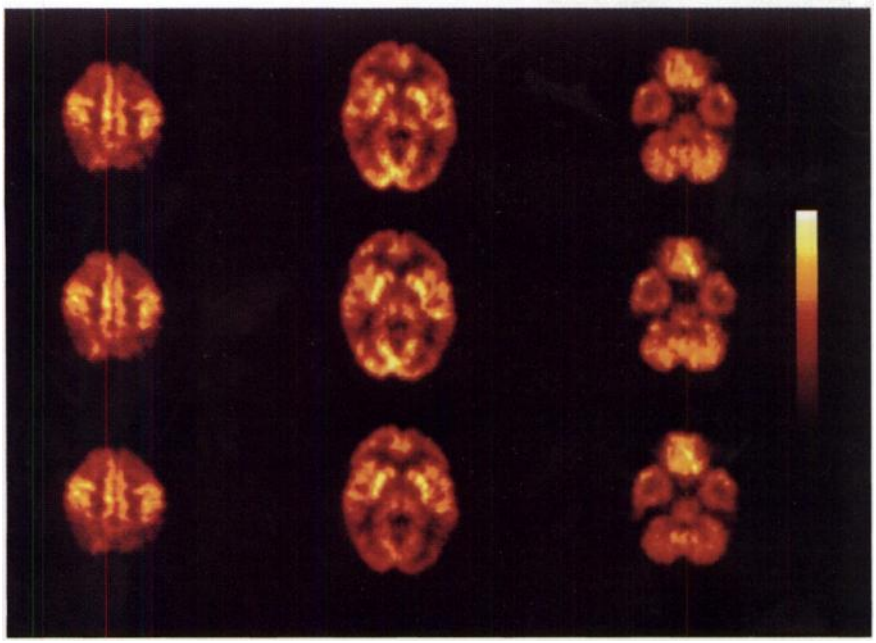

FIGURE 5. Representative images from a 55-yr-old woman with dementia showing three methods of AC. Top row, AC_{pre}; middle row, PIT_{sim} and bottom row, AC_{calc}. There is good agreement between PIT_{sim} and AC_{pre}, but AC_{calc} images show reduced glucose metabolism in occipital association cortex and cerebellum and increased metabolism in inferior frontal lobes.

equivalent to a second-degree polynomial in x, y and z directions, and Seitz et al. (*19*) reported that there was no significant effect on the integrity of the transformed voxel data in PET regional cerebral blood flow (rCBF) measurements. They also reported that the differences in quantification due to fitting PET rCBF data to the standard atlas were in the range of background noise.

The preinjection and postinjection transmission scans were performed 70 min apart, and it is possible that patient movement occurred between transmission measurements. We used a head restraint for each study and measured the degree of misregistration, retrospectively, using a voxel-based image coregistration package (*16*) to verify that movement was less than the voxel dimensions in all but 2 of the 26 patients. In these two cases, translations slightly greater than the interslice spacing were recorded in the Z direction, and all other movements were subvoxel. Thus, we believe that patient motion had a minimal effect on the accuracy of our measurements.

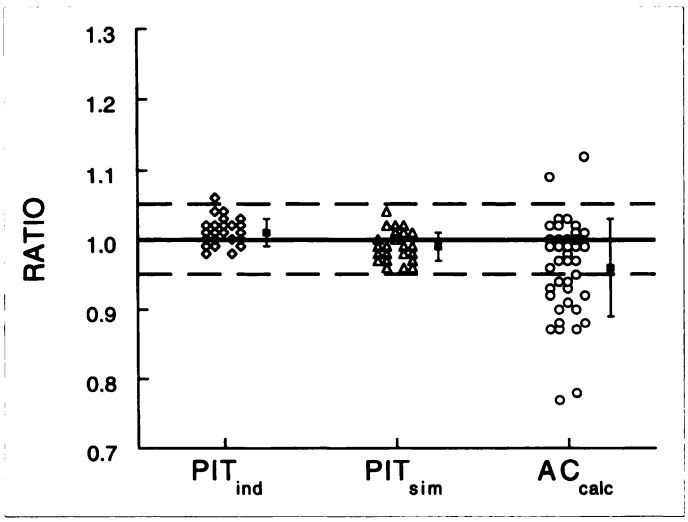

FIGURE 6. LCMRGlu ratios obtained in 44 brain regions using three methods of AC by comparison with AC_{pre}. Ratios shown are PIT_{ind}:AC_{pre} (diamonds), PIT_{sim}:AC_{pre} (triangles) and AC_{calc}:AC_{pre} (circles). Horizontal dashed lines indicate a discrepancy from AC_{pre} of ±5%. Error bars indicate 1 s.d. from the mean (shown as a square).

Finally, the scatter contribution to the preinjection and postinjection transmission measurements was different because sinogram windowing was not used for the preinjection scans. Thus, the attenuation coefficients for the preinjection transmission scan are broad beam and those for the postinjection scans are approximately narrow beam. We compensated for this difference by applying a narrow-to-broad-beam correction to the PIT scans, assuming a linear relationship between broad- and narrow-beam measurements. Previously published data (*12*) support this assumption over the range of tissue densities and thicknesses encountered in the brain. Our correction resulted in comparable attenuation correction factors for both the preinjection and postinjection techniques. We do not routinely use scatter correction for our emission data, although correction methods have been reported, because we believe that these methods are not fully validated for routine use (*23,24*). Therefore, it is appropriate to use broad-beam attenuation coefficients for our emission data. In PET centers, where emission scatter correction is routinely performed, the windowed PIT measurements can be used directly.

CONCLUSION

We validated PIT measurements for AC against the accepted preinjection transmission method and calculated AC in 26 patients. An alternative method for processing PIT data was included in the assessment that does not use information from an independent emission scan to estimate contamination of the PIT measurement. We found that both PIT methods yield accurate quantitative measurements of LCMRGlu. Calculated AC offers the greatest reduction in study duration; however, we believe that this method introduces unacceptable errors for LCMRGlu values (up to 23%) in cortical regions adjacent to thick bones or sinuses. In addition to shortening study duration and increasing patient throughput, our PIT_{sim} method has the advantages that (a) it is not affected by tracer redistribution and can therefore be applied to tracers other than FDG, including those with rapid in vivo kinetics and (b) it can be implemented

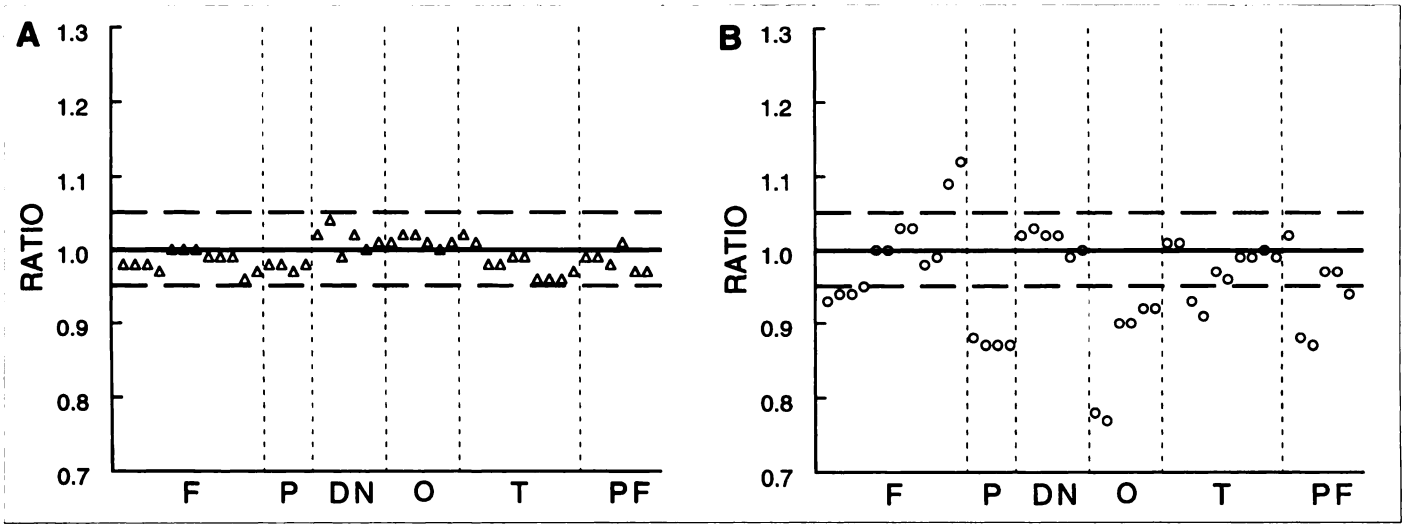

FIGURE 7. LCMRGlu ratios plotted by brain region for PIT_{sim} (A) and AC_{calc} (B) compared with AC_{pre}. Abbreviations on the abscissa refer to the following brain regions: frontal (F), parietal (P), deep nuclei (DN), occipital (O), temporal (T) and posterior fossa (PF). Horizontal dashed lines indicate a discrepancy from AC_{pre} of ±5%.

on commercially available PET devices without hardware modification.

ACKNOWLEDGMENTS

We gratefully thank Dr. Richard Fawdry and Mr. David Henderson from the PET chemistry section of the National Medical Cyclotron, where the [^{18}F]FDG was produced for patient studies; Kim Silver and Matthew Ayers for technical assistance in the collection of patient studies; Professor P.J.V. Beumont, Department of Psychiatry, University of Sydney, for permission to use the Computerized Brain Atlas Program in analysis of data presented in this report; Bill Jones from CTI PET Systems for supplying rod windowing hardware and for assistance with implementation and Dr. Lennart Thurfjell from the Center for Image Analysis, Uppsala University, Uppsala, Sweden, for maintenance of the Computerized Brain Atlas Program.

REFERENCES

1. Huang SC, Hoffman EJ, Phelps ME, Kuhl DE. Quantitation in positron emission tomography: 2. effect of inaccurate attenuation correction. *J Comput Assist Tomogr* 1979;3:804–814.
2. Dahlbom M, Hoffman EJ. Problems in signal-to-noise ratio for attenuation correction in high resolution PET. *IEEE Trans Nucl Sci* 1987;34:288–293.
3. Sokoloff L, Reivich M, Kennedy C, et al. The (^{14}C)-deoxyglucose method for the measurement of local cerebral glucose utilization: theory, procedure and normal values in the conscious and anesthetized albino rat. *J Neurochem* 1977;28:897–916.
4. Bergstrom M, Litton J, Eriksson L, Bohm C, Blomqvist G. Determination of object contour from projections for attenuation correction in cranial positron emission tomography. *J Comput Assist Tomogr* 1982;6:365–372.
5. Carson RE, Daube-Witherspoon ME, Green MV. A method for postinjection PET transmission measurements with a rotating source. *J Nucl Med* 1988;29:1558–1567.
6. Daube-Witherspoon ME, Carson RE, Green MV. Postinjection transmission attenuation measurements for PET. *IEEE Trans Nucl Sci* 1988;35:757–761.
7. Ranger NT, Thompson CJ, Evans AC. The application of a masked orbiting transmission source for attenuation correction in PET. *J Nucl Med* 1989;30:1056–1068.
8. Carroll LR, Kretz P, Orcutt G. The orbiting rod source: improving performance in PET transmission correction scans. In: Esser PD, ed. *Emission computed tomography—current trends*. New York: Society of Nuclear Medicine; 1983:235–247.
9. Huesman RH, Derenzo SE, Cahoon JL, et al. Orbiting transmission source for positron emission tomography. *IEEE Trans Nucl Sci* 1988;NS-35:735–739.
10. Thompson CJ, Dagher A, Lunney DN, Strother SC, Evans AC. A technique to reject scattered radiation in PET transmission scans. *Proc SPIE* 1986;671:244–253.
11. Meikle SR, Bailey DL, Hooper PK, et al. Simultaneous emission and transmission (SET) measurements for attenuation correction in whole-body PET. *J Nucl Med* 1995; 36:1680–1688.
12. Bailey DL, Meikle SR. A convolution-subtraction scatter correction method for three-dimensional PET. *Phys Med Biol* 1994;39:411–424.
13. Jones WF, Digby WM, Luk WK, Casey ME, Byars LG. Optimizing rod window width in positron emission tomography. *Conference record of the 1992 IEEE medical imaging conference*. Orlando; 1992:982–984.
14. Phelps ME, Huang S-C, Hoffman EJ, Selin C, Sokoloff L, Kuhl DE. Tomographic measurement of local cerebral glucose metabolic rate in humans with ^{18}F-2-fluoro-2-deoxy-D-glucose: validation of method. *Ann Neurol* 1979;6:371–388.
15. Huang SC, Phelps ME, Hoffman EJ, Sideris K, Selin CJ, Kuhl DE. Noninvasive determination of local cerebral metabolic rate of glucose in man. *Am J Physiol* 1980;238:E69–E82.
16. Eberl S, Kanno I, Fulton RR, et al. Automatic three-dimensional spatial alignment for correcting interstudy patient motion in serial PET studies. *Brain PET '93*. Akita, Japan; 1993:419–426.
17. Bohm C, Greitz T, Kingsley D, Berggren B, Olsson L. Adjustable computerized stereotaxic brain atlas for transmission and emission tomography. *AJNR Am J Neuroradiol* 1983;4:731–733.
18. Greitz T, Bohm C, Holte S, Eriksson L. A computerized brain atlas: construction, anatomical content, and some applications. *J Comput Assist Tomogr* 1991;15:26–38.
19. Seitz RJ, Bohm C, Greitz T, et al. Accuracy and precision of the computerized brain atlas programme for localization and quantification in positron emission tomography. *J Cereb Blood Flow Metab* 1990;10:443–457.
20. Thurfjell L, Bohm C, Greitz T, Eriksson L. Transformations and algorithms in a computerized brain atlas. *IEEE Trans Nucl Sci* 1993;40:1187–1191.
21. Palmer MR, Rogers JG, Bergstrom M, Beddoes MP, Pate BD. Transmission profile filtering for positron emission tomography. *IEEE Trans Nucl Sci* 1986;33:478–481.
22. Meikle SR, Dahlbom M, Cherry SR. Attenuation correction using count-limited transmission data in positron emission tomography. *J Nucl Med* 1993;34:143–150.
23. Bergstrom M, Eriksson L, Bohm C, Blomqvist G, Litton J. Correction for scattered radiation in a ring detector positron camera by integral transformation of the projections. *J Comput Assist Tomogr* 1983;7:42–50.
24. Shao L, Karp JS. Cross-plane scattering correction—point source deconvolution in PET. *IEEE Trans Med Imag* 1991;10:234–239.